Multi-mode-fiber compatible WDM/WDDM with an ultra-large wavelength dynamic range

Ray T. Chen, Jian Liu, and Xuegong Deng

Microelectronics Research Center
Department of Electrical and Computer Engineering
University of Texas at Austin
Austin, Texas 78758

ABSTRACT

In this article, wavelength division multiplexing (WDM) devices suitable for multi-mode-fiber-based networks are presented. A packaged wavelength division demultiplexer (WDDM) is demonstrated first at wavelengths of 750 nm, 780 nm, 810 nm, and 840 nm. The insersion losses are 8.28 dB, 9.41 dB, 6.78 dB, and 11.71 dB, respectively. The reduction of wavelength separation from 30 nm to 2 nm is achieved using a beveled-edge to couple optical signals into a waveguiding plate. A path-reversed substrate-guided wave holographic interconnection is employed for a WDDM with a channel wavelength spacing as small as 2 nm. A waveguide grating with a 45^{o} incident angle and a 45^{o} diffraction angle is fabricated using 20 μm thick DuPont photopolymer film HRF 600x001. The dispersion and the 3 dB bandwidth of the device are measured to be 0.18^{o}/nm and 20 nm, respectively. A four-channel wavelength demultiplexing is demonstrated at 796 nm, 798 nm, 800 nm, and 802 nm with no crosstalk observed. A one-to-five cascaded 4-channel WDDM with ± 5% energy uniformity under an s-polarization is also demonstrated to increase the user-sharing capacity. Twenty fanout channels (5x4) are experimentally achieved. Its potential application for dense WDM at 1555 nm is also addressed. Time-reversal of the demonstrated devices automatically provides the WDM function.

Keywords: wavelength division multiplexing; volume holographic grating; photopolymer films; optical interconnects; dispersion.

1.0 Introduction

In optical communications, wavelength division multiplexing (WDM) is employed as a powerful approach to significantly increase the capacity of the fiber transmission lines. At the end of a transmission line, a WDDM is always employed to separate optical channels of different wavelengths and to route optical signals to their designated users. For long haul telecommunications at wavelengths of 1330 nm and 1550 nm, investigators have been primarily focusing on two kinds of grating-based approaches. They are arrayed waveguide gratings (AWG)[1-6], and fiber Bragg gratings [7-11]. The dispersion of the AWG is caused by the length differences of the arrayed waveguides. The wavelength selectivity of a fiber Bragg grating is due to a relatively long fiber grating with a small refractive index modulation. In data communications, where interconnection distance is relatively short, usually within 1 km, it is intended to use short wavelengths, for example

800 nm, in conjunction with a multimode fiber to transmit optical signals. In this scenario, optical transceivers are mature and the aggregate bandwidth can meet the system requirements[12-16].

In section 2.0, the authors present a packaged 4-channel wavelength division demultiplexer (WDDM) which has the required stability and compactness for a system integration. In section 3.0, a novel dispersion-enhanced WDDM structure using a path-reversed substrate-guided-wave configuration working at a center wavelength of 800 nm is presented. Thease devices are intended to be used in data communications, where interconnection distance is relatively short, usually within 1 km. To further reduce the wavelength separation at 1555 nm, a path-reversed WDDM with a 2nm channel spacing is demonstrated, and the result is shown in section 3.0 as well. The concluding remarks is provided in section 4.0.

2.0 Packaging of a wavelength division demultiplexer

The designed WDDM demultiplexes four channels of 750 nm,780 nm, 810 nm, and 840 nm. The demonstrated system is shown in Figure 2.1 where the layout of our design

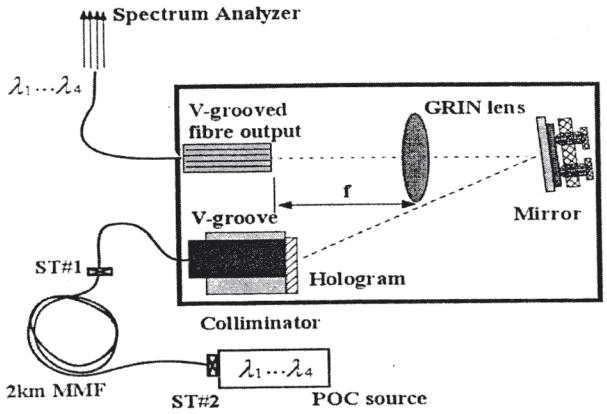

Figure 1. Schematic illustration of the wide WDDM and the test setup.

and testing setup are illustrated. The 20μm thick hologram is recorded on a DuPont photopolymer layer[10]. For a small deviation δλ from the central wavelength λ_c, the diffraction angle relative to the surface normal direction outside the hologram is[11, 14]

$$\theta(\lambda) = \arcsin(n \sin(\theta_g + \delta\lambda/\lambda_c \tan \theta_g)), \quad (1)$$

where θ_g is the diffraction direction for λ_c inside the gratings, and n is the corresponding optical refraction index. Therefore,the directions of the diffracted beams outside the hologram vary almost linearly with the deviations of the wavelength, which results in

equally spaced channels. After reflection, the demultiplexed beams are focused via a plano-convex GRIN lens of focal length 18mm. The lens has an open aperture of 9 mm. The spacing between two neighbor fibers in the V-groove is 250 μm. For n = 1.512, λ_c = 795nm, the grating angle determined by using Eq.(1) is θg = 0.23 rad.

The collimator with ST fiber connector, the mirror and mount, the GRIN lens, and the V-grooved fibers are integrated. The measured diffraction efficiency of the hologram at 800nm is 60%.

To maintain the accuracy during the packaging, a monitoring system is setup by using a CCD and an imaging lens. Each component is carefully positioned on the base in the propagation order of the optical signals through the system. The spacing of the diffracted beams on the focal plane are determined and in good agreement with Eq. (1). The last step is coupling the demultiplexed signals into the four V-grooved multimode fibers. The process is carried out with two optical stages totally having four degrees of freedom (X-Y-Z-θ). The demultiplexed beams focused on the end of the V-grooved fibers are clearly monitored during the coupling process. We first place a thin metal pin around the focal plane of the GRIN lens. Shown in Figure 2.2, the pin is slightly moved so that the focused spots are blocked. Then, bring the V-grooved fibers just along the pin is shown without touching it. The focused spots can be seen on the end of the V-grooves where the alignment pin is removed. Simultaneously, input optical signal to two of the four fibers by using laser diodes. Bringing the demutiplexed beams to coincide with the fiber ends, further coupling is carried out with spectrum analyzer. The two signals of 750 nm and 840 nm coming out of two of the four V-grooved fibers are illustrated in Figure 2.3.

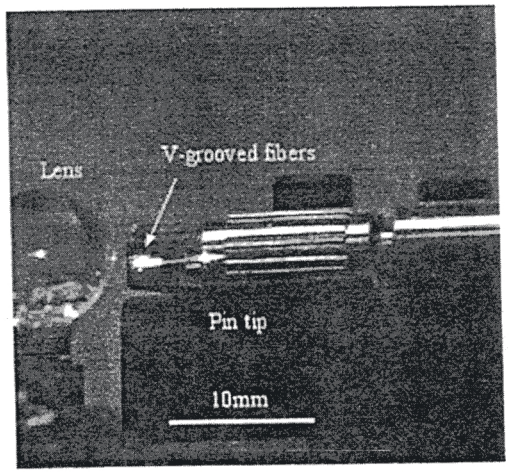

Figure 2.2 Packaging wide WDDM device. Coupling demultiplexed beams to the V-grooved fibers by using a thin metal pin. The focused spots on the fiber ends can be seen in the picture.

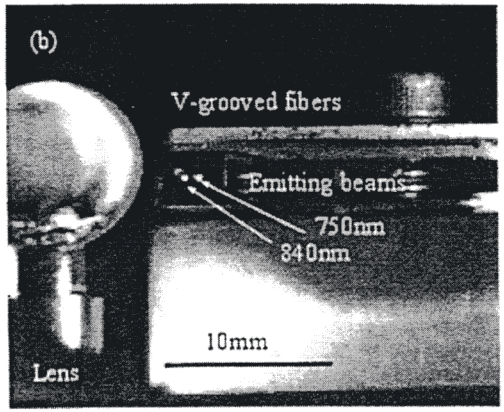

Figure 2.3. Packaging wide WDDM device. Monitoring the positions of the focused beams on the end of V-grooves. The emitting bright spots from two fibers can be clearly seen.

The collimator, hologram, mirror and GRIN lens are reliably integrated on to the designed package. We have carefully monitored the four output signals before and after we permanently fixed all discrete component onto the package housing. Figure 2.4 shows the output signals before and after the permanent packaging. The pictures confirm that the WDDM has the desired mechanical stability.

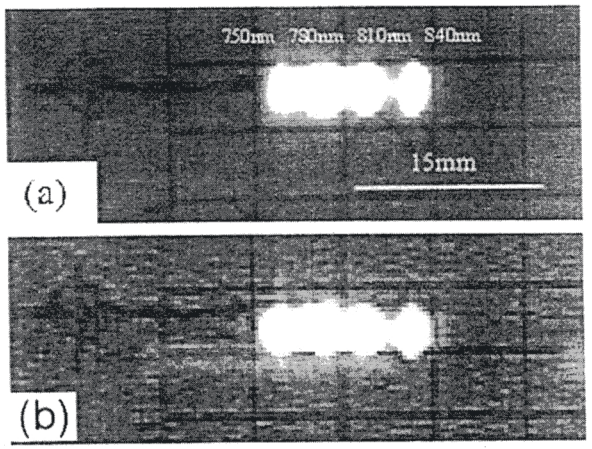

Figure 2.4. (a) Images of the demultiplexed optical signals before permanently fixed the discrete components unto the housing. (b) Images of the demultiplexed optical signals two days after. All images are taken *in situ*. No displacements of the components have been observed.

The test results of this WDDM device are summarized in Table 2.1. The insertion losses are measured to be 8.28 dB, 9.41 dB, 6.78 dB, and 11.71 dB, respectively. The system insertion losses, including the input ST connector, collimator, hologram, mirror, lens, and the output V-gooved fibers, seem high[15] because the wavelengths of the source signal have a center wavelength deviation up to 9.0 nm. Besides, the spectrum widths of the source signals are measured and listed as $\Delta\lambda$ (full width at -6dB peak power). The spacing of the diffracted beams is not uniform and their positions shift accordingly. The biggest displacement of the spacing is more than 40 μm at the focal plane. For a single channel, say, 750 nm, the measured insertion loss could be as low as -2.3dB. However, to achieve a balanced 4-channel output, there exists some tradeoffs among these channels. The relatively high losses and cross-talk levels are due to the deviation of the wavelength of the four lasers from the designed. Channel 1 and Channel 4 have much less cross-talks of < -24 dB. The wide spectrum distribution also accounts for the strong cross-talks among channel 3 and channel 4. We confirmed these analysis. Using an Ar^+ laser pumped Ti:Sapphire tunable laser, we measured the cross-talks of the device for the designated wavelengths. The results are listed in Table 2.2. Typical values are less than -30 dB. However, there is no significant improvement on the insertion losses.

Table 1: Summary of the characteristics of the WDDM.

Channel	λ_i^0 (nm)	λ_i^e (nm)	$\Delta\lambda$ (nm)	δx_f (μm)	Insertion Loss (dB)	Cross talks (dB)			
						1	2	3	4
1	750	756.5	1.38	53.8	8.28		-24.6	--#	--
2	780	789.0	3.28	74.7	9.41	-15.3		-23.7	--
3	810	814.3	2.24	35.4	6.78	--	--		-14.4
4	840	844.0	3.62	33.4	11.7	--	--	--	

λ_i^0 indicates the wavelengths of the designated channels, while those of the output from the POC source are denoted by λ_i^e. $\Delta\lambda$ is used to represent the -6dB spectrum width. δx_f is the calculated shift of the focused spots from the designed position.
There is no cross-talk or the value is too weak and essentially beyond the range of the spectrum analyzer.

Table 2.2: Calibration of the WDDM by using a Ti:Sapphire laser.

Channel	λ_i^e (nm)	$\Delta\lambda$ (nm)	Cross talks (dB)*			
			1	2	3	4
1	750.0	<0.2		-32.0	--#	-41.0
2	780.0	<0.2	-43.2		--	-35.4
3	810.0	<0.2	<-42.0	<-35.0		<-39.0
4	840.0	<0.2	-36.1	-26.1	--	

Wavelengths of the Ti:Sapphire laser are denoted by λ_i^e. $\Delta\lambda$ is used to represent the -6dB spectrum width.
*The cross-talks from 810nm are typically less than -35.5dB. Due to the fluctuations of the output at this wavelength are not completely measured, concrete data could not be presented here.
There is no cross-talk or the value is too weak and essentially beyond the range of the spectrum analyzer.

Figure 2.5 shows the output spectrum from the four-channel v-grooved fibers when input optical signals are at wavelengths 756.5 nm, 789.0 nm, 814.3 nm, and 844.0 nm. Note that the lasers we employed are low-cost CD lasers from Sharp. Cross-talks can be significantly reduced to the levels shown in Table 2.2 when other commercial available lasers such as DFB lasers, vertical surface emitting lasers (VCSEL), and external cavity semiconductor lasers. Other related interesting work implies that our work is of potential application [21]. Recent research on the differential mode of multimode fibers such as Ref. 22 may push the deployment of multi-mode fiber further to the front of data communications.

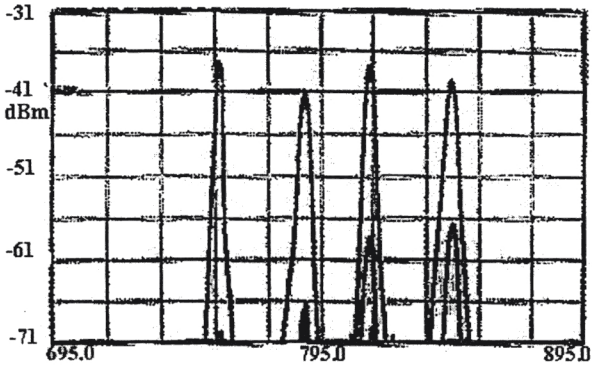

Figure 2.5. Output spectrum from the four-channel V-grooved fibers of the demultplexed POC signal. The four channels of POC source are at 756.5nm, 789.0nm, 814.3 nm, 844.0nm, respectively.

3.0 A path-reversed substrate-guided-wave approach for a dense WDDM

For previous substrate-guided-wave holograms [23, 24], optical signals of various wavelengths are dispersed by an input holographic grating, propagating within a wagveguiding plate with total internal reflection (TIR), and then coupled out of the substrate by output holographic gratings. The interchannel wavelength separation of such a WDDM is totally dependent on the length between the input and the output couplers. To obtain a smaller channel wavelength spacing, employment of a long substrate is a necessity. Meanwhile, a lens array is always needed to couple the output optical signals with different wavelengths into a fiber array. In our proposed path-reversed substrate-guided-wave optical interconnects, instead of using an input holographic grating, a beveled edge is used to couple optical signals into the waveguiding plate with an angle larger than the critical angle of the plate, and a DuPont photopolymer-based holographic grating is employed to separate the optical signals of different wavelengths. It is a path-reversed structure because the optical signals are dispersed by the output waveguide

hologram. The input light comes from the waveguiding plate and the diffracted light goes into the air. Only one lens is used to couple the dispersed optical signals into their designated fibers. Moreover, multiple fanouts can be realized by integrating a cascaded holographic grating array on the same waveguiding plate.

3.1. Working principles

3.1.1 Photopolymer films

DuPont (DuPont Holographic Materials, Wilmington, Delaware, USA) provides promising holographic film due to its dry processing, long shelf life, good photospeed, and large index modulation[25-28]. The holographic photopolymer is usually coated from solvent onto a clear support, typically Mylar polyester film. A removable cover sheet is used as a protecting cover. The thicknesses of photopolymer are available from 10 to 100 μm. The hologram formation mechanism in the photopolymer films is known to be a three-step process. First, an exposure initiates the interference pattern, which causes initial polymerization and diffusion of the monomer molecules to bright fringe areas from the dark fringe neighborhoods in the photopolymer. A higher concentration of polymerization means a higher refractive index. Second, a uniform UV light is required for dye bleaching and complete polymerization. Third, a baking process can further enhance the refractive index modulation of the hologram formed in the photopolymer film. It is shown that the dynamic properties of diffraction efficiency versus exposure time can be controlled by the two recording beam intensities, which are related with the polymerization rates and the diffusion rates in the photopolymer films[26]

3.1.2 Dispersion and bandwidth of the path-reversed substrate-guided-wave holograms

Fig. 3.1(a) shows the structure of the proposed path-reversed substrate-guided-wave interconnect scheme. Collimated optical signals with different wavelengths are coupled into a waveguiding plate with an Aluminum-coated beveled edge of an angle α, zig-zagging within the substrate with a bouncing angle larger than the critical angle of the waveguiding plate, and then coupled out by the photopolymer-based volume holographic grating fabricated on one side of the substrate. The dispersed optical signals can be coupled by a focusing-lens into a fiber array. The thickness of the waveguiding plate is t. Fig. 3.1(b) shows the detailed structure of the volume holographic grating with a thickness of d. The grating has a period of Λ and a slanted angle of ϕ. The grating equation is given by[19]

$$\Lambda_y (sin\theta_2' + sin\theta_2) = m\lambda / n, \quad m = 0, \pm 1, \pm 2, \ldots\ldots \qquad (3.1)$$

where θ_2 and θ_2' are the incident and the diffraction angles of the optical signals in the holographic grating region at the center wavelength of λ (in the air), respectively. n is the average refractive index of the holographic grating region. $\Lambda_y = \Lambda / sin\ \phi$ is the grating period projected in Y direction. m represents the mth order for forward diffraction. In our case, m is equal to 1. Let θ_{diff} be the designed diffraction angle in the air of refractive index n_3 and θ the bouncing angle, i.e., the incident angle at the interface between the waveguiding plate and the grating. From the shown geometry of the beveled edge, we have $\theta = 2\alpha$.

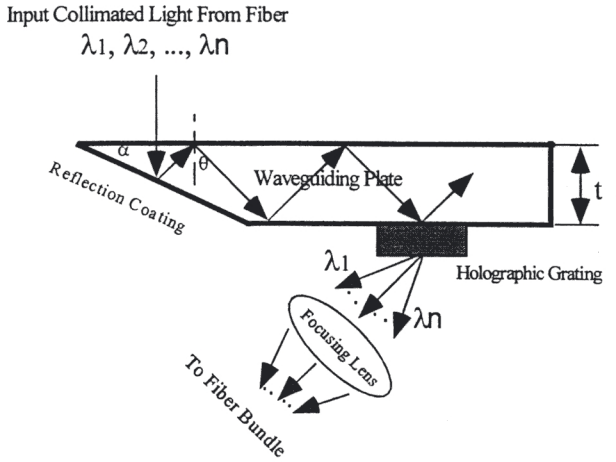

(a)

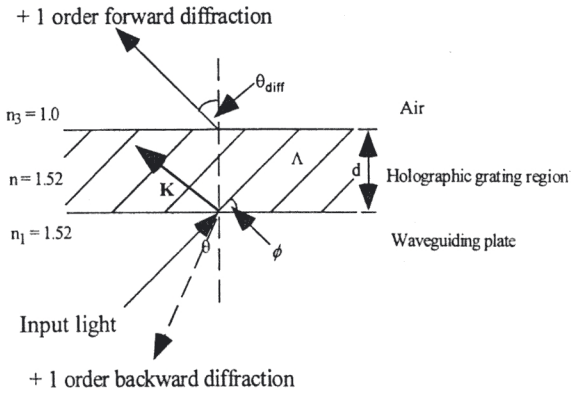

(b)

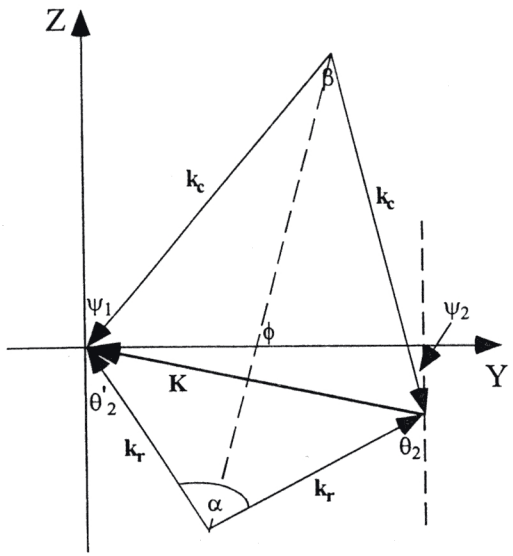

(c)

Figure 3.1 A path-reversed substrate-guided wave optical interconnection. (a) structure; (b) guided-wave holographic grating; (c) phase-matching condition for recording and reconstruction of the grating.

The dispersion of the grating can be derived by differentiating Eq. (3.1), which gives

$$d\theta_{diff} / d\lambda = sin\phi / \Lambda\, cos\theta_{diff} = n\,(sin\theta_2' + sin\theta_2) / \lambda cos\theta_{diff}, \qquad (3.2)$$

From the geometry of Fig. 3.1 (c), the slanted angle ϕ of the grating and the grating period Λ are given by

$$\phi = \pi / 2 + (\theta_2' - \theta_2) / 2; \qquad (3.3)$$

and

$$\Lambda = \lambda / 2\, n\, sin\,[(\theta_2' + \theta_2) / 2]. \qquad (3.4)$$

respectively, in which θ_2' and θ_2 are calculated from the designed values of θ_{diff} and θ using the Snell's Law.

Fig. 3.2(a) plots grating dispersion as a function of diffraction angle at incident angles of 0^o, 30^o, 45^o, 60^o, and 75^o by using Eq. (3.2) at center wavelength of 800 nm. Incident angles of 0^o and 30^o are plotted in Fig. 2 for comparison. The thickness of the guided-wave holograpgic gratings is 20 μm. The refractive indices are $n_1 = 1.0$, $n = n_3 = 1.52$. It is clearly indicated that higher dispersion occurs for a grating with a larger incident angle and a larger diffraction angle.

In design of a WDDM using a dispersion grating, the spectral bandwidth $\Delta\lambda$ of the grating has to accommodate all wavelength channels demultiplexed. The approximate spectral bandwidth is given by Ludman[29] in the form of

$$\Delta\lambda / \lambda = \Lambda\, cos\,\theta_2'\, sin\,\phi / d\, sin\,\theta_2'. \qquad (3.5)$$

which is plotted in Fig. 3.2 (b). Table 1 shows the calculated parameters for four guided-wave grating structures. There exists a trade-off between the dispersion and the bandwidth of the guided-wave holographic gratings.

3.1.3 Hologram recording parameters

Fig. 3.1(c) shows the phase matching diagram for all the wavevectors in the holographic medium. The recording wave vector $\mathbf{k_c}$ ($|\mathbf{k_c}| = 2\pi n' / \lambda_c$) are phase-matched with the grating vector $\mathbf{K}$ ($|\mathbf{K}| = 2\pi / \Lambda$), and so does the reconstruction wave vector $\mathbf{k_r}$ ($|\mathbf{k_r}| = 2\pi n / \lambda$) and $\mathbf{K}$. n' is the average refractive index of the guided-wave holographic emulsion at recording wavelength λ_c. From the geometry of Fig. 3.1(c), the recording

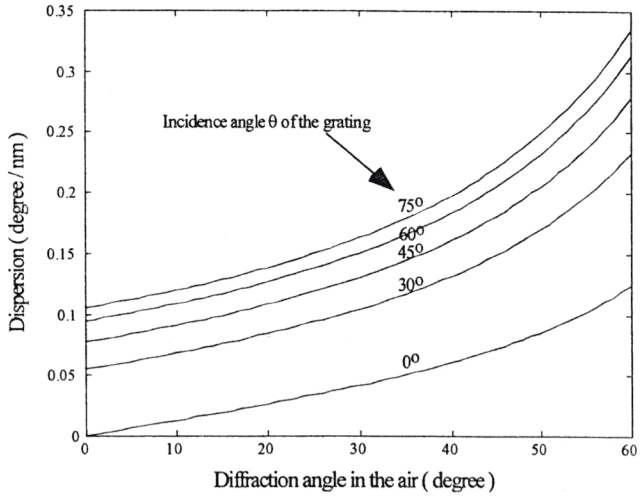

(a)

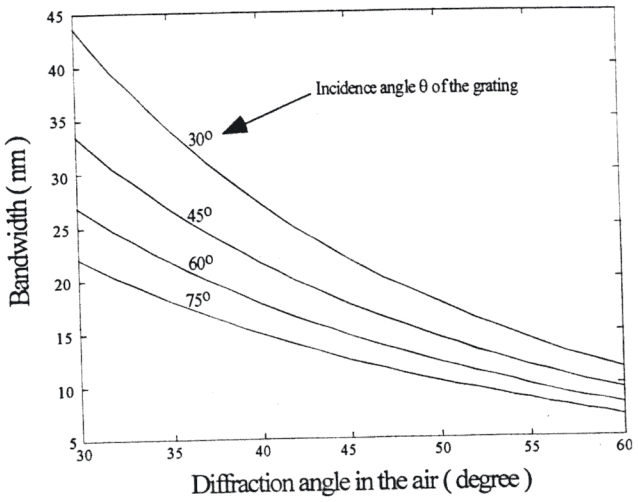

(b)

Figure 3.2 (a) Dispersion calculated by Eq. (3.2); (b) bandwidth calculated by Eq. (3.5).

angles in the hologram medium of the two recording beams at wavelength λ_c are derived and given by

$$\Psi_1 = \pi / 2 - (\phi - \beta / 2), \qquad (3.6)$$

and

$$\Psi_2 = (\phi + \beta / 2) - \pi / 2. \qquad (3.7)$$

where

$$\beta = 2\, sin^{-1}\{(n\,\lambda_c / n'\lambda)\, sin[(\theta_2' + \theta_2) / 2]\}, \qquad (3.8)$$

which is the angle between two recording beams. Note that the phase matching condition in Fig. 3.1(c) is in the holographic medium. In practice, the recording angles calculated by Eqs. (6) and (7) must be converted into those angles in the air by the Snell's Law.

It is obvious that the absolute values of the two recording angles in the air can not be over 90^o. Otherwise, a prism or other higher index medium must be used in the recording process. To justify the proposed approach, numerous cases are simulated and four cases are summarized in Table 3.1. Among the four cases shown in Table 3.1, case 2 has a reasonably high dispersion, and an acceptable bandwidth. Moreover, this kind of

structure is easy to be fabricated. Note that the working principle presented herein is not only suitable for 800 nm but also for 1300 and 1550 nm. Both 800 nm and 1555 nm are presented in section 3.2.

Table 3.1 Parameters of four guided-wave holographic gratings

Case	α	θ	θ_{diff}	Λ	ϕ	$d\theta_{diff} / d\lambda$	B.W.
1	22.5	45	30	495.2	77.1	0.13	33
2	22.5	45	45	444.6	81.4	0.18	18
3	22.5	45	60	411.2	84.9	0.28	9.4
4	30	60	60	358.3	77.4	0.31	8.1

Note: all angles are in degree and grating period and wavelength are in nm. B.W. stands for bandwidth.

3.2. Experiment

3.2.1 WDDM working in the 800 nm region

We use a 514 nm Argon ion laser to record the output holographic grating. The reconstruction wavelength is designed to be at 800 nm. A Ti: Saphire tunable laser is employed to characterize the performance of the device. DuPont photopolymer film HRF 600x001-20 with a thickness of 20 μm is chosen to record the guided-wave holographic grating. The waveguiding plate has a thickness of 6.3 mm. The beveled angle α is 22.5^o, and the diffraction angle θ_{diff} in the air is 45^o.

In our experiment, +1 order backward diffraction is observed to be about 15% of the intensity of the +1 order forward diffraction, which can be interpreted by the rigorous coupled wave analysis (RCWA)[30], as conceptually depicted in Fig. 3.3. The decomposed space-harmonic components of total field in the grating region allowed to be coupled into the glass plate region (backward diffraction) and the air (forward diffraction) include a +1 order forward diffraction and a +1 order backward diffraction. Other diffraction orders are cutoff outside the grating region. It is shown from Fig. 3.3 that backward diffraction orders always exist as long as forward diffraction orders exist, because of larger refractive index in region 1 (waveguiding region). The existing +1 order backward diffraction takes a certain percentage of input energy. This part of energy might be used for on-site channel monitoring of the WDDM.

Fig. 3.4 shows the measured dispersion of the WDDM. Theoretical results calculated by Eq. (3.2) are also shown in the figure as solid line. It is obvious that the experimental results are consistent with the theoretical expectations. The dispersion is found to be insensitive to the states of input polarization. Fig. 3.5 gives the measured diffraction efficiencies of the +1 order forward diffraction as a function of wavelength under different states of polarization. The diffraction efficiency is defined as the intensity of the

+1 order forward diffraction divided by the intensity of the optical signal entering the WDDM device (not the output waveguide grating). Actually, before the optical signal impinges on the grating, it experiences losses of Fresnel reflection at the air-glass and the reflection-coating interfaces, and absorption and scattering of the waveguiding glass plate. Therefore, the actual diffraction efficiencies of the grating are larger than those given in Fig. 3.5. The 3dB bandwidth of this device is determined to be 20 nm, which is close to that given in Table 3.1. The discrepancy of the diffraction efficiencies between p- and s- polarization states shows this device is polarization sensitive. Theoretical analysis by the rigorous coupled wave analysis will be given in later publications.

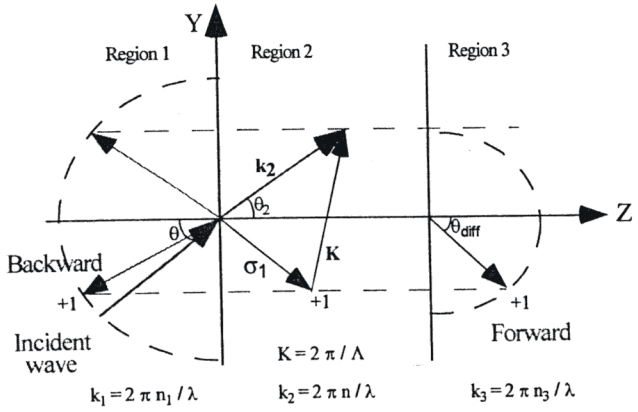

Figure 3.3 Conceptual interpretation of forward and backward diffractions by rigorous coupled wave analysis.

Fig. 3.6 is an experimental result of a four-channel WDDM operating at 796 nm, 798 nm, 800 nm, and 802 nm, for which the bandwidth of the device can accommodate all the four-channel, as shown in Fig. 3.5, while maintaining a 2 nm wavelength separation. This image is taken by a CCD camera from the focal plane of a lens with a focal length of 20 cm. From Fig. 3.6, we can see that the four-channel are totally separated. There is no crosstalks observed in our experiment. Using an aspheric lens, it is possible to focus the light beams much smaller and to couple them into standard fiber bundles/arrays.

3.2.1.1 A path-reversed substrate-guided-wave optical interconnect with multiple fanouts

To further increase the capacity and reduce the cost, we design a path-reversed substrate-guided-wave based WDDM with a multi-fanout feature. Fig. 3.7 shows that N cascaded volume holographic gratings are integrated on the same waveguiding plate, and the optical signals with different wavelengths are zig-zagged within the plate and coupled sequentially out of the substrate by the cascaded gratings. For each individual fanout, the dispersed wavelengths can be focused and coupled into optical fiber arrays. If each

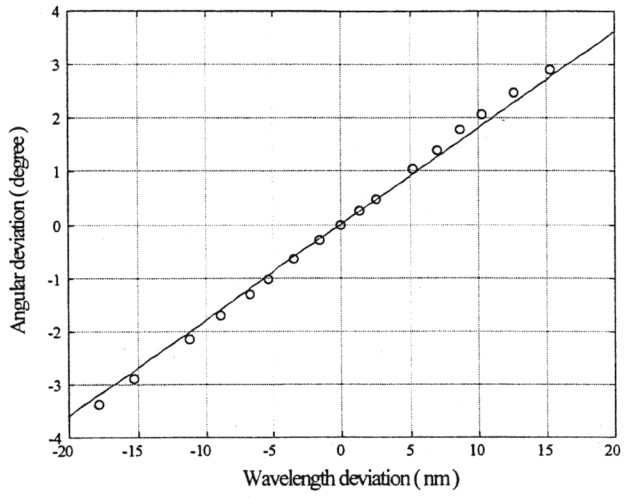

Figure 3.4 Experimental results (o) and theoretical expectations (solid line) of anglar deviation as a function of wavelength change at center wavelength of 800 nm.

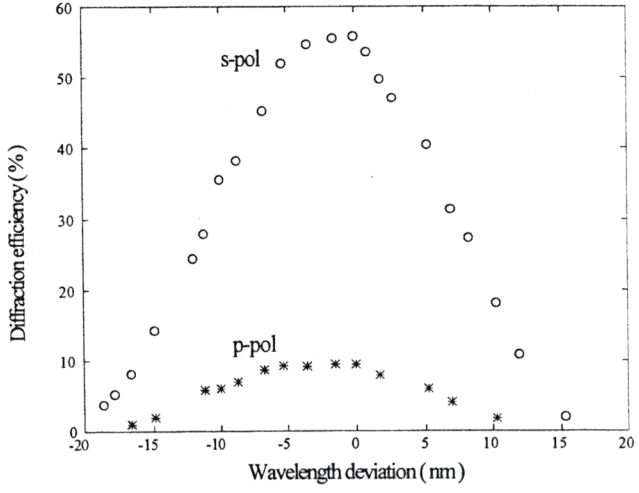

Figure 3.5 Measured diffraction efficiency as a function of wavelength deviation at the center wavelength of 800 nm under an s-wave and a p-wave.

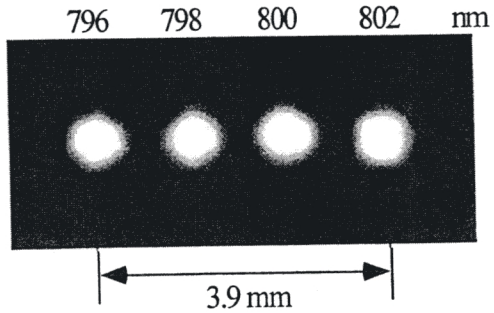

Figure 3.6 A CCD image of the light spots for this WDDM operating at 796 nm, 798 nm, 800 nm, and 802 nm.

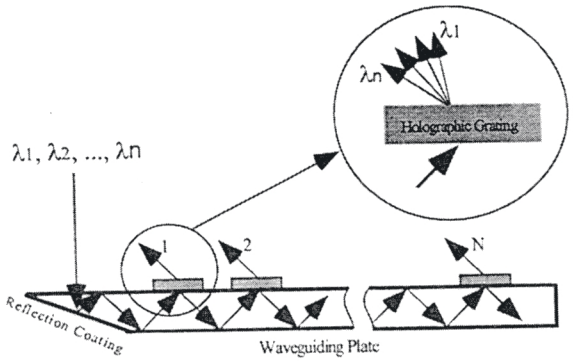

Figure 3.7 A path-reversed substrate-guided wave optical interconnection with multi-fanouts for WDDM application

holographic grating is capable of separating M wavelengths, such a WDDM has a channel capacity of NxM, N times larger than that described in last section. One important issue relating this device is to obtain a uniform fanout energy distribution, which can be found elsewhere[31-35].

Using the same grating parameters as mentioned before, and a beveled waveguiding plate with a thickness of 3.2 mm, five cascaded holograms are sequentially recorded on the same substrate by using DuPont photopolymer film HRF 600 with a thickness of 20

μm. Fig. 3.8 shows a CCD image of the device operating at center wavelength of 800 nm under an s-polarization. A three-dimensional intensity profile is also given in Fig. 8(b). Fanout energy distribution uniformity is measured to be within ± 5%. For each individual fanout, four-channels with a channel wavelength separation of 2 nm are also obtained as those shown in Fig. 6. With this large user sharing capability, the device is promising for data communications.

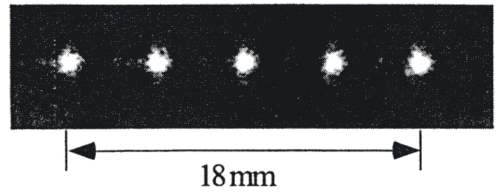

(a)

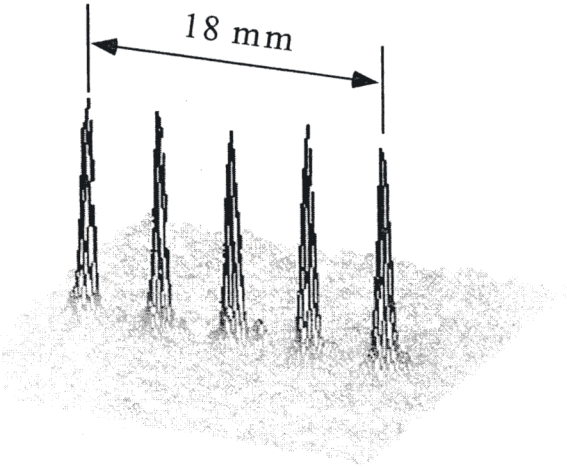

(b)

Figure 3.8 Experimental results of a one-to-five fanout WDDM operating at center wavelength of 800 nm. (a) CCD image; (b) 3-D intensity profile.

3.2.2 WDDM working in the 1555 nm region

Figure 3.9 gives simulation results of dispersion and bandwidth as a function of diffraction angle in the air for the path-reversed holographic WDDM working at a center wavelength of 1555 nm at different incident angles. Figure 3.10 is an experimental result of a four-channel WDDM operating at 1551 nm, 1553 nm, 1555 nm, and 1557 nm. This image is taken by a CCD camera from the focal plane of a lens with a focal length of 20 cm. By tuning the laser wavelength from 1551 to 1557, we can see clearly the spot movement. The diffraction efficiency is measured to be 14% at 1555 nm. The relatively large spot size is due to the poor quality of the collimation. The spot size can be reduced to diffraction limit when appropriate collimating optical elements are employed.

It is possible to select a configuration with a large dispersion and an acceptable bandwidth to achieve standard 100 GHz channel spacing without degrading the TEM_{00} mode quality and adding more complexity to the system. Detailed investigation and experimental results will be presented in the conference.

4.0 Discussion and conclusion

A low-cost packaging of a wavelength division demultiplexer (WDDM) is demonstrated at wavelengths of 750 nm, 780 nm, 810 nm, and 840 nm. This packaging is of potential to be used in short distance data communications. The insersion losses are 8.28 dB, 9.41 dB, 6.78 dB, and 11.71 dB, respectively.

A novel multi-wavelength photopolymer-based path-reversed substrate-guided-wave optical interconnect is presented to reduce the wavelength separation down to 2 nm. Both 800 nm and 1555 nm band can be realized using the proposed idea. The dispersion and the bandwidth of the guided-wave holograms are analyzed. It is shown that by adjusting the incident angle and the diffraction angle of the path-reversed structure the dispersion can be enhanced. Incident angle larger than the critical angle of the substrate can be obtained by beveling one edge of the waveguiding plate. The bulky waveguiding glass plate provides mechanical and environmental robustness. As the dispersion occurs for the output holographic grating, the TEM_{00} mode profile of the dispersed optical signals with different optical wavelengths is well-retained, and this also reduces the difficulties in integration with fiber array/bundles.

In our experiment, DuPont photopolymer film HRF 600x001-20 (20 μm thick) is chosen to record the holographic grating. The beveled angle of the waveguiding plate is $\alpha = 22.5^{o}$, and the diffraction angle of the holographic grating in the air is designed to be at 45^{o}. The measured dispersion results are consistent with the theoretical analyses and are polarization-insensitive. A bandwidth of 20 nm is obtained for such a polarization-sensitive device (in terms of diffraction efficiency). A four-channel WDDM separating wavelengths of 796 nm, 798 nm, 800 nm, and 802 nm is demonstrated with no channel crosstalk. Furthermore, this structure can incorporate with cascaded hologram arrays to obtain multiple fanouts for increasing the user-sharing capacity and reducing the cost of the device. A one-to-five fanout WDDM is fabricated with energy fluctuation within $\pm$ 5% under an s-polarization at center wavelength of 800 nm. It is promising for this path-reversed substrate-guided-wave optical interconnect to be used as WDDM in data communications.

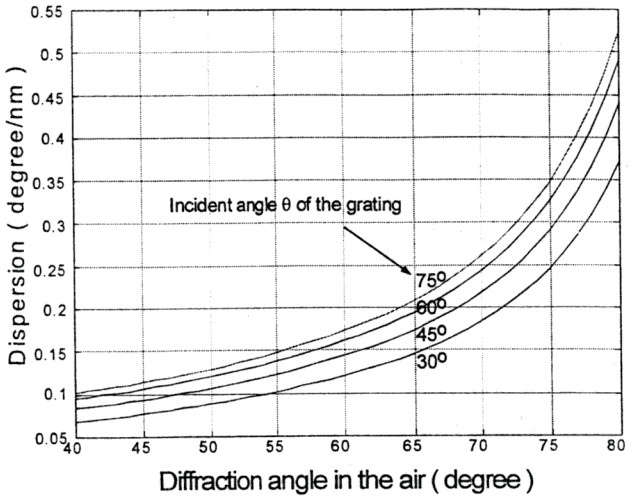

(a)

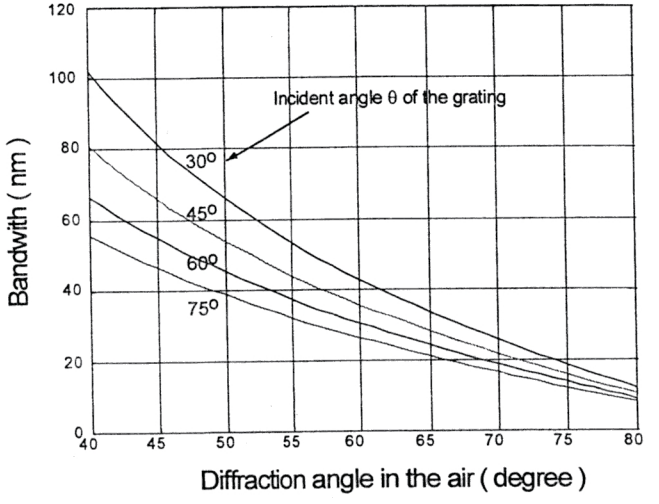

(b)

Figure 3.9 Dispersion (a) and bandwidth (b) of the path-reversed holographic WDDM operating at a center wavelength of 1555 nm.

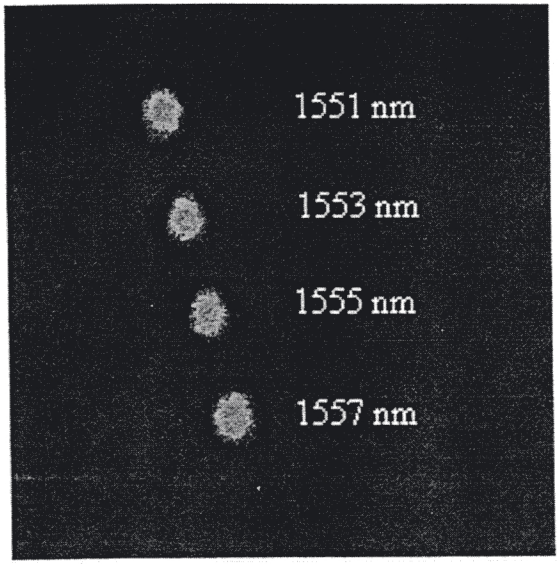

Spot movement direction →

Figure 3.10 Experiment of four channel WDDM working in the 1555 nm region. The spot distance between 1551 nm and 1557 nm is ~ 2 mm.

A four channel WDDM centered at 1555 nm with wavelength separation of 2 nm is further demonstrated using the path-reversed substrate-guided-wave approach. It is possible to select a configuration with a large dispersion and an acceptable bandwidth to achieve standard 100 GHz channel spacing without degrading the TEM_{00} mode quality and adding more complexity to the system. Detailed investigation and experimental results will be presented in the conference.

Acknowledgments: This research is supported by Ballistic Missile Defense Organization, Army SSDC, the Center of Optoelectronics Science and Technology (COST), DARPA, Office of Naval Research, AFOSR, Cray Research, DuPont, Lightpath, 3M Foundation, RRI, and the Advanced Technology Program (ATP) of the state of Texas.

References:

1. M. K. Smit, "New focusing and dispersive planar component based on an optical phased array," Electron. Lett. **24**, 385-386 (1988).

2. H. Takahashi, S. Suzuki, K. Kato, and I. Nishi, "Arrayed-waveguide grating for wavelength division multi/demultiplexer with nanometer resolution," Electrn. Lett. **26**, 87-88 (1990).

3. C. Dragon, C. H. Henry, I. P. Kaminow, and R. C. Kistler, "Efficient multichannel integrated optics star coupler on silicon," IEEE Photon. Technol. Lett. **1**, 241-243 (1989).

4. C. Dragon, "An NxN optical multiplexer using a palnar arrangement of two star couplers," IEEE Photon. Technol. Lett. **3**, 812-815 (1991).

5. C. Dragon, C. A. Edwards, and R. C. Kistler, "Integrated optics NxN multiplexer on Silicon," IEEE Photon. Technol. Lett. **3**, 896-899 (1991).

6. M. K. Smit and C. van Dam, "PHASAR-based WDM devices: principles, design and applications," IEEE J. Selected Topics in Quantum Electron. **2**, 236-250 (1996).

7. K. O. Hill, Y. Fujii, D. C. Johnson, and B. S. Kawasaki, "Photo-sensitivity in optical fiber waveguides: application to reflection filter fabrication," Appl. Phys. Lett. **32**, 647-649 (1978).

8. B. S. Kawasaki, K. O. Hill, D. C. Johnson, and Y. Fujii, "Narrow-band Bragg reflectors in optical fibers," Opt. Lett. **3**, 66-68 (1978).

9. F. Bilodeau, D. C. Johnson, S. Theriault, B. Malo, J. Albert, and K. O. Hill, "An all-fiber dense-wavelength-division multiplexer/demultiplexer using photoimprinted Bragg gratings," IEEE Photon. Technol. Lett. **7**, 388-390 (1995).

10. I. Baumann, J. Seifert, W. Nowak, and M. Sauer, "Compact all-fiber add-drop-multiplexer using fiber Bragg gratings," IEEE Photon. Technol. Lett. **8**, 1331-1333 (1996).

11. K. O. Hill and G. Meltz, "Fiber Bragg grating technology fundamentals and overview," J. Lightwave Technol. **15**, 1263-1276 (1997).

12. G. W. Neudeck, J. Denton, J. D. Schaub, R. Li, C. L. Schow, and J. C. Campbell, "A high speed Si photodiode by epitaxial lateral growth," The 56th Annual Device Research Conference Digest, Charlottesville, Virginia, June 22-24, 1998.

13. C. Schow, J. Schaub, R. Li, J. Qi, and J. C. Campbell, "A 1Gb/s monolithically integrated Silicon NMOS optical receiver," To be published in IEEE Quantum Electronic Devices, 1998.

14. S. Hu, J. Ko, and L. A. Coldren, "High-performance densely packed vertical-cavity photonic integrated emitter arrays for direct-coupled WDM applications," IEEE Photon. Technol. Lett. 10, 766-768 (1998).

15. D. L. Huffaker and D. G. Deppe, "Multiwavelength, densely packed 2x2 vertical-cavity surface-emmitting laser array fabricated using selective oxidation," IEEE Photon. Technol. Lett. 7, 858-860 (1996).

16. S. Y. Hu, J. Ko, O. Sjolund, and L. A. Coldren, "Optical crosstalk in monolithically-integrated multiple wavelength vertical-cavity laser arrays for multimode WDM local area networks," Electron. Lett. 34, 676-678 (1998).

17. W.J. Gambogi, A.M. Weber, and T.J. Trout, ``Advances and Applications of DuPont Holographic Photopolymers", SPIE, 2043,2-13,(1993)

18. C.C. Zhou, Z.H. Fu, R. T. Chen, B.M. Davies, ``Dispersion Correction of Surface-normal Optical Interconnection Using Two Compensated Holograms", Applied Physics Letters, 72(25), 3249-3251,(1998)

19. R. R. A. Syms, *Practical Volume Holography*, Clarendon Press (Oxford, 1990).

20. For W(D)DM working with multimode fibers, typical insertion loss is 3dB, intensity extinction ratio (cross-talk) are better than 20dB.See, for example, H.F. Mahlein, ``Fiber-Optic Communication in the Wavelength-Division Multiplex Mode", Fiber and Integrated Optics, 4, 339-372,(1983).

21. Alec MacGregor, John Fox, Terry Giles, ``Bandwidth reduction in high speed laser-based communications systems over MMF and bandwidth recovery through laser transmitter mode conditioning", Optical Engineering, (to be published) December,1998

22. Casmimer DeCusatis, John Fox, Terry Giles, ``Differential mode delay in gigabit fiber optic links", OSA 1998 Annual Meeting, Baltimore, MD

23. M. M. Li and R. T. Chen, "Five-channel surface-normal wavelength-division demultiplexer using substrate-guided waves in conjunction with a polymer-based littrow hologram," Opt. Lett. **20**, 797-799 (1995).

24. Y. K. Tsai, Y. T. Huang, and D. C. Su, "Multiband wavelength-division demultiplexing with a cascaded substrate-mode grating structure," Appl. Opt. **34**, 5582-5588 (1995).

25. W. Gambogi, K. Steijn, S. Mackara, T. Duzik, B. Hamzavy, and J. Kelly, "HOE imaging in DuPont holographic photopolymers," Proc. SPIE **2152**, 282-293 (1994).

26. U. Rhee, H. J. Caulfield, C. S. Vikram, and J. Shamir, "Dynamics of hologram recording in DuPont photopolymer," Appl. Opt. **34**, 846-853 (1995)

27. S. Piazzolla and B. K. Jenkins, "Holographic grating formation in photopolymers," Opt. Lett. **21**, 1075-1077 (1996).

28. H. J. Zhou, V. Morozov, and J. Neff, "Characterization of DuPont photopolymers in infrared light for free-space optical interconnects," Appl. Opt. **34**, 7457-7459 (1995).

29. J. E. Ludman, "Approximate bandwidth and diffraction efficiency in thick holograms," Am. J. Phy. **50**, 244-246 (1982).

30. T. K. Gaylord and M. G. Moharam, "Analysis and applications of optical diffraction by gratings," Proc. IEEE 73, 894-937 (1985).

31. Jian Liu and Ray T. Chen, "Substrate-guided-wave-based optical interconnects for multi-wavelength routing and distribution networks," To be published in J. Lightwave Technol. 1999.

32. T. Nakaya, Y. Katoh, T. Kubota, and M. Tabeda, "Diffraction efficiency of a grating coupler for an array illuminator," Appl. Opt. 35, 3891-3898 (1996).

33. Jian Liu, Chunhe Zhao, R. Lee, and Ray T. Chen, "Cross-link optimized cascaded volume hologram array with energy-equalized one-to-many surface-normal fan-outs," Opt. Lett. **22**, 1024-1026 (1997).

34. Jian Liu, Zhenhai Fu, Ray T. Chen, "Polarization sensitivity of photopolymer-based volume holograms for one-to-many surface normal optical interconnects," Opt. Eng. **37**, 660-665 (1998).

35. Jian Liu and Ray T. Chen, "A two-dimensional dual-wavelength routing network with 1-to-10 cascated fanouts," IEEE Phton. Technol. Lett. **10**, 238-240 (1997).